Direct measurement of Ne-Mg-Si nuclei in cosmic rays with DAMPE

Elisabetta Casilli,[a,b,*] **Corrado Altomare,**[c] **Paolo Bernardini,**[a,b]
Francesco de Palma,[a,b] **Essna Ghose**[a,b,†] **and**
Antonio Surdo[b] **on behalf of the DAMPE Collaboration**

[a]*Dipartimento di Matematica e Fisica E. De Giorgi, Università del Salento, I-73100 Lecce, Italy*

[b]*Istituto Nazionale di Fisica Nucleare (INFN) - Sezione di Lecce, I-73100, Lecce, Italy*

[c]*Istituto Nazionale di Fisica Nucleare (INFN) - Sezione di Bari, I-70125, Bari, Italy*

E-mail: elisabetta.casilli@le.infn.it

A precise measurement of the cosmic-ray spectra provides important information on their origin, acceleration and propagation processes in the Galaxy. The Dark Matter Particle Explorer (DAMPE) is a satellite-based cosmic-ray experiment that has been operational for more than 7 years. Since its launch in December 2015, it is continuously collecting data on high-energy cosmic particles with very good statistics and particle identification capabilities, thanks to a large geometric factor and a good charge resolution. In this contribution, the direct measurement of the intermediate mass cosmic rays is presented, in particular the observation of the cosmic-ray Ne, Mg and Si nuclei, which are thought to be mainly produced and accelerated in astrophysical sources.

ICRC2023
38th International Cosmic Ray Conference
The Astroparticle Physics Conference

---

*Speaker

†National PhD Program in Space Science and Technology, University of Trento (Italy).

1. Introduction

Cosmic Rays (CRs) are high-energy particles of Galactic or extragalactic origin, containing key information about the astrophysical sources that generated them, and the interstellar medium they travel through. Over the past years, several experiments revealed special features in the CR spectra, consisting in unexpected deviations from the single power-law behavior predicted by shock acceleration mechanisms for protons, helium and heavier nuclei below 3-4 PeV (the so-called *knee* of the all-particle spectrum) [1–3]. In order to understand these spectral features, a deep analysis of the intermediate mass nuclei like Ne, Mg and Si is necessary, above all in those high-energy regions (>1 TeV/n) which cannot be reached by spectrometer-type experiments, neither by balloon-borne detectors affected by considerable statistical and instrumental uncertainties [4–6]. In this work the analysis procedure for the measurement of the Ne, Mg and Si energy fluxes observed by DAMPE is presented, showing the event selection criteria adopted to properly identify them. Finally, some preliminary Ne and Mg results are also shown, as early efforts of the ongoing analysis toward the measurement of the energy spectra.

2. The DAMPE instrument

The DArk Matter Particle Explorer (DAMPE) [7] is a space-borne particle and gamma-ray detector, designed to investigate several scientific fields, such as the observation the CR spectra up to ~10 TeV for the electromagnetic component ($\gamma, e^{\pm}$) and hundreds of TeV for protons and nuclei, while searching for indirect signatures of dark matter. The instrument consists of four sub-detectors: a plastic scintillator detector (PSD), a silicon-tungsten tracker-converter (STK), a bismuth germanium oxide (BGO) calorimeter, and a neutron detector (NUD). The PSD is made by 82 bars, divided into two orthogonal planes in the *Y* and *X* views, each composed by two layers of staggered bars. It is designed to discriminate charged particles from gamma rays, and to measure their absolute charge. The STK is used to measure the track of the particles inside the detector, and to convert photons in $e^{\pm}$ pairs with the help of tungsten layers. The BGO calorimeter is made of 14 layers, with 22 bars each, for a total depth of ~32 radiation lengths and ~1.6 nuclear interaction lengths. Its main goal is to measure the energy of the particles and separate hadronic from electromagnetic showers. Finally, the NUD is composed of boron-loaded plastic scintillators, and allows a better discrimination between the electromagnetic and hadronic particles.

3. Data sample

In this work, 79 months of flight data collected by DAMPE in the period between January 2016 and July 2022 are analyzed. The satellite operations are affected by an instrumental dead time, equals to ~17.2% of the total operation time, while ~1.7% is dedicated to the on-orbit calibrations. Moreover, all the events collected by the detector while crossing the South Atlantic Anomaly (SAA) region (~4.9%) are excluded. By taking into account all these information, the resulting live time is $\sim 1.6 \times 10^8$ s, corresponding to ~76% of the total operation time. Monte Carlo (MC) simulation data are generated using the GEANT4 toolkit [8] with the FTFP_BERT physics list for Ne and Mg nuclei in the primary energy range from 100 GeV to 500 TeV, with a smooth transition to the EPOS-LHC physics list for particles with energy > 10 TeV/n.
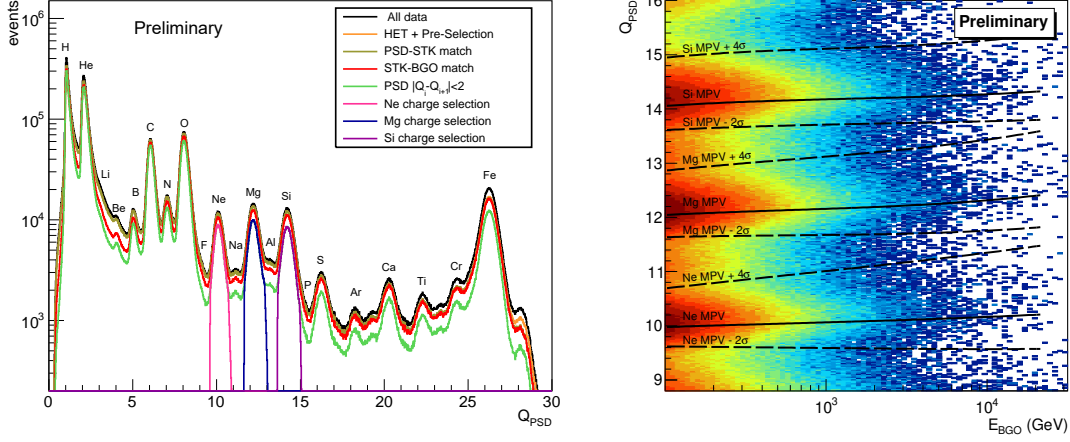
4. Event selection

4.1 Pre-selection

Some *pre-selection* criteria are applied to the data in order to select only the well reconstructed events. First of all, we require the activation of the High Energy Trigger (HET), which occurs when the energy deposition in the first three BGO layers is greater than ~10 Minimum Ionizing Particles (MIPs) and higher than ~2 MIPs in the fourth layer (1 MIP$_{BGO}$ ~23 MeV). Moreover, in order to avoid the geomagnetic cut-off effect, the events with a total energy deposition inside the BGO calorimeter (E_{BGO}) lower than 100 GeV are excluded. Then, we ask for events with top-down development of the shower, by requiring that the energy deposited in the first two BGO layers is lower that the energy released in the third and fourth layers. Finally, in order to ensure a good shower containment, most of the side events are excluded from the analysis by requiring the BGO crystal with the maximum energy deposition in the first three layers not to be at the edge of the calorimeter, and the maximum energy deposited in a single layer to be less than 35% of E_{BGO}.

4.2 Track selection

The trajectory of the incident particle is selected among the multiple STK tracks reconstructed with the Kalman filter algorithm, by jointly considering the number of hits on the track, the χ^2/dof value, and the deviation between the track and the shower axis inside the calorimeter. In order to ensure a good match between the STK and both the PSD and BGO hits, the selected track is then required to pass inside some given PSD and BGO fiducial volumes, in particular through the entire length of the calorimeter.

4.3 Charge selection

The particle charge reconstruction is performed by using the PSD hits along the selected track, by exploiting their direct proportionality to the square root of the energy loss by ionization. The PSD can provide, at most, four independent charge measurements, one for each sub-layer. A detailed charge reconstruction algorithm is applied for each hit based on its ionization energy deposition, including the path length correction, the light attenuation correction and the light yield saturation correction. Moreover, for a reliable PSD charge evaluation, a further consistency cut is imposed, by requiring that the difference between the charge Q of two subsequent layers satisfies $|Q_i - Q_{i+1}|<2$ (with $i = 0, \ldots, 3$, sub-layer by sub-layer, from the top to the bottom of the PSD). In this way, the global charge value (Q_{PSD}) is obtained as the average between the charge measurements of the PSD layers which satisfy the consistency requirement described above. It should be noted that this average involves at least two different measurements, since we require the presence of at least one charge value for the *Y* and *X* PSD views. On the *left* panel of Fig.1, we report the spectrum of the PSD global charge for the on-orbit data at different selection steps, from the pre-selection cuts up to the charge selection of the Ne, Mg and Si candidates. This last selection is performed by fitting the Q_{PSD} distribution in different BGO energy ranges with a *LanGaus* function, obtained by the convolution of a Landau with a Gaussian distribution. The Most Probable Values (MPVs) and sigma values extrapolated from the fit are then used to implement the energy-dependent charge selection ranges represented by the dashed lines reported on the *right* panel of Fig.1, as a function of the BGO energy.

Figure 1: Spectrum of the PSD global charge (Q_{PSD}) at different selection steps (on the *left*), and as a function of E_{BGO} (on the *right*), where the preliminary charge selection ranges for Ne, Mg and Si candidates are represented with the dashed lines.

5. Contamination estimation

The charge selection of Ne, Mg and Si candidates may include a contamination from other elements, in particular from the intermediate Na and Al nuclei. A preliminary measurement of this background can be evaluated by using the on-orbit data, with the application of a multi-Gaussian fit (given by the sum of 5 Gaussian distributions) for Ne, Na, Mg, Al and Si, and with the application of a single Gaussian fit for O and F, as reported in Fig.2. In this way, the contamination is estimated as the fraction of the Gaussian area of the closer elements inside the multi-Gaussian distribution, for the given charge selection range. The resulting background is found to be ∼ 6.5% for Ne due to O, F and Na, ∼ 8.2% for Mg due to Na and Al, and finally ∼ 2.4% for Si due to Al, while the background contributions from other elements are negligible. These results represent a preliminary estimation of the background contamination levels. A more detailed procedure will be applied when a complete set of MC simulations (including all the elements involved in the analysis) will be available.

6. Selection efficiencies

6.1 High Energy Trigger efficiency

The HET efficiency can be estimated by means of another trigger implemented in DAMPE, the Low Energy Trigger (LET), which requires an energy deposition greater than ∼0.4 MIPs in the first two BGO layers, and higher that ∼2 MIPs in the third and fourth layers (a more inclusive trigger with respect to the HET). We compute the HET efficiency in the following way:

$$\varepsilon_{HET} = \frac{N_{HET|LET}}{N_{LET}} \tag{1}$$
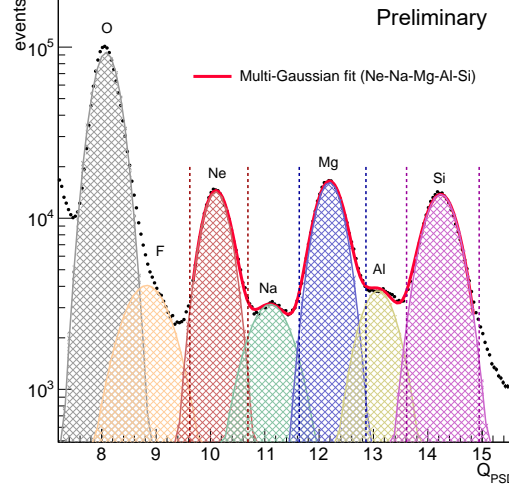
Figure 2: Preliminary measurement of the background, obtained using the flight data (black dots). A multi-Gaussian fit (given by the sum of 5 Gaussians) is applied to Q_{PSD}. The single Gaussian distributions, extrapolated from the fit, are represented by colored shaded areas for Ne (red), Na (green), Mg (blue), Al (yellow) and Si (violet), while the single Gaussian fits for O and F are represented in gray and orange, respectively. The vertical dashed lines represent the charge selection ranges for the Ne, Mg and Si candidates.

where $N_{HET|LET}$ is the number of candidate events activating both the HET and LET triggers, while N_{LET} is the number of LET events. On Fig.3 we present the HET efficiency as a function of E_{BGO}, computed for the Ne and Mg samples, and both for on-orbit data and MC simulations. The resulting difference between flight and MC data is found to be within 2%, showing a good agreement.

6.2 Charge reconstruction efficiency

An evaluation of the charge reconstruction efficiency for the Q_{PSD} global charge can be carried out using the charge measurement provided by the two PSD layers (Q_Y and Q_X), as follows:

$$\varepsilon_{PSD} = \frac{N_{Q_Y|Q_X|Q_{PSD}}}{N_{Q_Y|Q_X}} \tag{2}$$

where $N_{Q_Y|Q_X|Q_{PSD}}$ is the number of events selected by using the PSD global charge measurement and both the two separated PSD views, while $N_{Q_Y|Q_X}$ is the number of events selected by the combined charge measurements of just the Y and X layers of the PSD (considered separately). The results show that the agreement between on-orbit data and MC simulations is within $\sim 3\%$.

7. Acceptance calculation

In this work, we use a sample of Ne and Mg simulated data for the evaluation of the detector effective acceptance. In particular, the acceptance at a given i-th bin of incident energy is calculated by using the following formula:

$$A_{\text{eff},i} = A_{\text{gen}} \times \frac{N_{\text{pass},i}}{N_{\text{gen},i}} \tag{3}$$
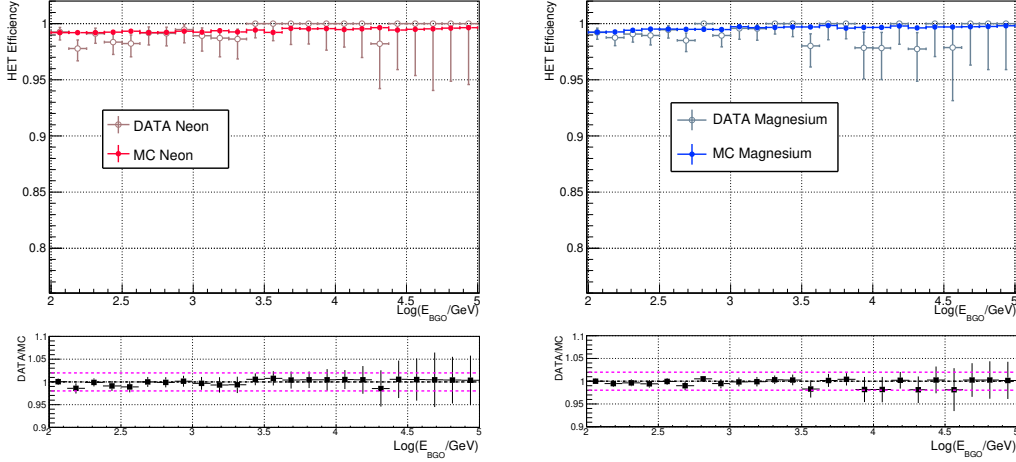
Figure 3: HET efficiencies for Ne (on the *left*) and Mg (on the *right*) as a function of E_{BGO}. The agreement between flight data (empty dots) and MC simulations (filled dots) is within $\sim 2\%$ for both Ne and Mg samples.
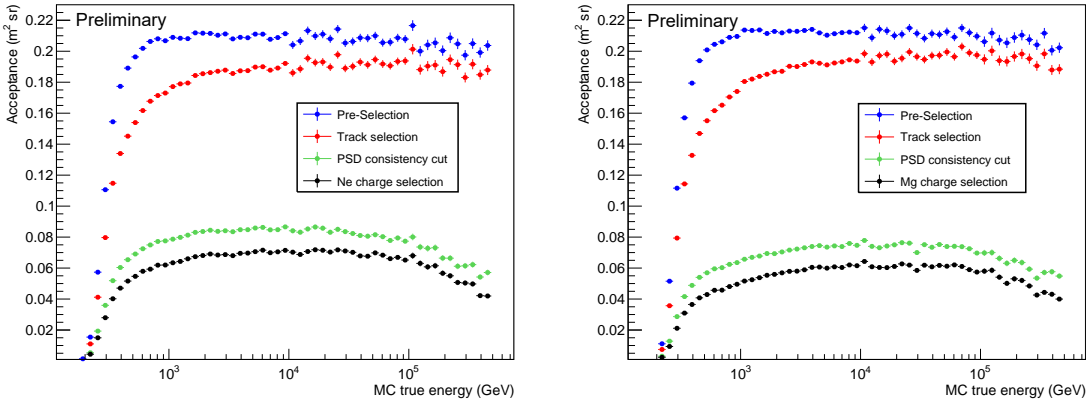
Figure 4: Preliminary effective acceptance as a function of the primary energy, for the Ne (on the *left*) and Mg (on the *right*) samples. Each different color represents an additional selection cut, up to the final cut in black, which represents the charge selection.

where A_{gen} is the geometrical factor used for MC simulations, $N_{pass,i}$ is the number of selected events in the i-th bin of primary energy, and $N_{gen,i}$ is the total number of generated events in the same energy bin. In Fig.4 the preliminary effective acceptance is shown as a function of the primary energy for Ne (on the *left*) and Mg (on the *right*), resulting from the application of different event selection criteria. It can be noted that the application of the PSD consistency cut produce a large reduction in the acceptance calculation, with an additional decrease clearly visible above 10^5 GeV. We are currently working on the improvement of the selection criteria, in order to ensure both a good charge reconstruction and a larger acceptance.
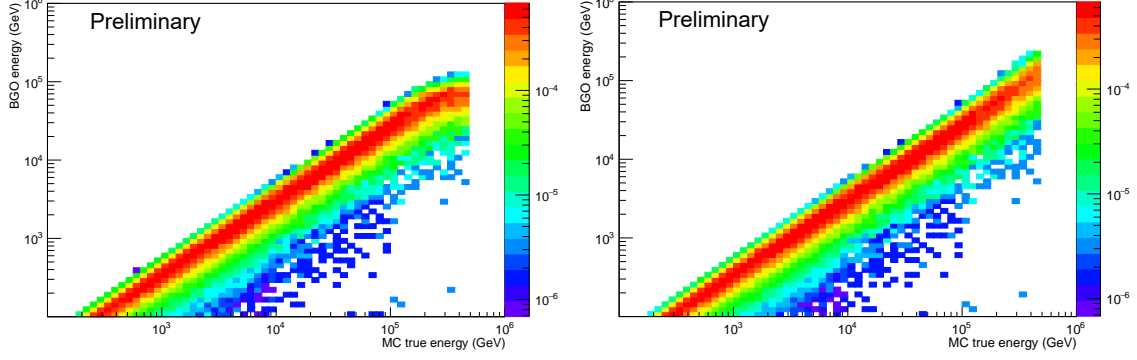
Figure 5: Response matrix derived from the Mg simulated data passing all the event selection criteria, before (on the *left*) and after (on the *right*) the application of the BGO saturation correction.

8. Unfolding procedure

Due to the limited thickness of the BGO calorimeter (see Section 2), the energy deposited by a CR particle represents only a fraction of its primary energy. In order to evaluate the CRs flux, it is necessary to unfold the detector response with the use of MC simulations. We employ a method based on the Bayes theorem [9], by requiring the MC events to pass the event selection criteria described above, and inferring the true energy of the incoming particle from the observations with the use of the following formula:

$$N_{\text{obs},i} = \sum_j M_{ij} \, N_{\text{true},j} \qquad (4)$$

where $N_{\text{obs},i}$ is the number of observed events in the i-th bin of BGO energy, $N_{\text{true},j}$ is the number of events in the j-th bin of primary energy, and M_{ij} is the energy response matrix, which represents the probability that an event with incident energy in the j-th bin is detected in the i-th bin of deposited energy. Moreover, two corrections are applied to the energy measurements. The first is based on the study of dedicated MC simulations, which reproduce the Birk's quenching effect that could occur inside the calorimeter [10], while the second consists in a method developed in order to correct the energy deposit in the events affected by the saturation of one or more BGO bars [11]. In Fig.5 the preliminary response matrix derived from the Mg simulations is shown, before (on the *left*) and after (on the *right*) the application of the saturation correction, whose effect is clearly visible above 100 TeV.

9. Conclusions and future perspectives

A detailed procedure for the direct measurement of Ne, Mg and Si in CRs with DAMPE has been described in this work. The various steps toward the measurement of the energy fluxes have been presented, although an improvement of the event selection criteria is still necessary for reliable results. This work is currently ongoing, together with the evaluation of all the systematic contributions and a more detailed analysis of the contamination from the close nuclei.

Acknowledgments

References

[1] Q. An et al. (DAMPE Collaboration), Sci. Adv. 5, eaax3793 (2019).

[2] F. Alemanno et al. (DAMPE Collaboration), Phys. Rev. Lett. 126, 201102 (2021).

[3] M. Aguilar et al. (AMS Collaboratio), Phys. Rep. 894, 1-116 (2021).

[4] H.S. Ahn et al., ApJ 707, 593-603 (2009).

[5] V. Grebenyuk et al., Adv. Space Res. 64, 12 (2019).

[6] M. Aguilar at al. (AMS Collaboration), Phys. Rev. Lett. 124, 211102 (2020).

[7] J. Chang et al. (DAMPE Collaboration), Astropart. Phys. 95, 6 (2017).

[8] S. Agostinelli et al., Nucl. Instrum. Methods Phys. Res., Sect. A 506, 250 (2003).

[9] G. D'Agostini, Nucl. Instrum. Meth. A 362, 487 (1995).

[10] J.B. Birks, Proc. Phys. Soc. London Sect. A 64, 875 (1951).

[11] C. Yue et al. Nucl. Instrum. Methods Phys. Res. Sect. A 984, 164645 (2020).

PoS(ICRC2023)115